

## Tunnelling close beneath an existing tunnel in clay – perpendicular undercrossing

C. Y. GUE\*, M. J. WILCOCK†, M. M. ALHADDAD†, M. Z. E. B. ELSHAFIE†, K. SOGA‡ and R. J. MAIR†

A series of centrifuge model tests in clay was carried out to investigate the response of an existing tunnel at different clear distances to new tunnelling. A three-dimensional (3D) staged tunnelling model was adopted to simulate a wide range of tail void volume losses for the new tunnel construction while monitoring detailed 3D soil surface settlements and tunnelling-induced strains in the existing tunnel lining. This paper also presents a detailed case study of a similar scenario in the London Underground redevelopment of Bond Street station; various state-of-the-art instrumentation methods, including fibre optic Brillouin optical time domain reflectometry, instrumented tunnel bolts and photogrammetry, were deployed to monitor the response of the existing Royal Mail tunnel due to the new tunnelling works close beneath. The combination of field and centrifuge modelling data provides important new insights into the deformation mechanisms encountered in such complex tunnelling scenarios.

KEYWORDS: centrifuge modelling; field instrumentation; tunnels & tunnelling

### INTRODUCTION

Tunnelling underneath an existing tunnel in close proximity is a common recurring problem in densely populated cities with underground transportation networks. Perpendicular undercrossing is of particular interest in this paper as it is more common than parallel piggy-back scenarios.

Kim (1996) conducted scaled  $1g$  laboratory testing of tunnelling interactions in Speswhite kaolin clay for perpendicular over- and undercrossing for normally consolidated clay with a fixed volume loss of 6.0%. Boonyarak (2014) carried out centrifuge testing of a perpendicular undercrossing in sand; this study modelled tail void volume loss in series of advancements at a fixed volume loss of 2.0% at two different clear distances. However, there is a knowledge gap for overconsolidated clay at various volume losses, prohibiting a generalised approach for analyses.

Conventional assessment methods mostly rely on numerical models without much understanding of the deformation mechanisms involved. This is especially true for cross-sectional bending strains, while the response of an existing tunnel in the longitudinal direction is often conservatively assumed to follow the greenfield vertical settlement profile.

In the longitudinal direction, Bracegirdle *et al.* (1996) included a reduction factor for the greenfield horizontal strain as a component of axial strain suggested by Attewell *et al.* (1986) for pipeline assessment, taking account of different pipe–soil stiffnesses and ratios of pipe diameter to trough width. However, these reduction factors are less practical for tunnels, given their significantly larger diameter.

Nonetheless, the approach proposed by Bracegirdle *et al.* (1996) assumed that the tunnel followed the greenfield settlement profile, which in itself was a conservative assessment. Klar *et al.* (2005) presented a closed-form Winkler spring solution (equation (1)) method for pipeline bending moment assessments, which was derived from typical transverse Gaussian settlements and considered the soil–pipe relative stiffness. Klar *et al.* (2005) proposed an alternative subgrade modulus analogue,  $K_s$ , in place of the method proposed by Vesic (1961), which suffered from disparity between elastic continuum and the Winkler solution for  $i_x/R < 10$ .

$$\frac{M_{\max} i_x^2}{E_1 I S_{\max}} = \sum_{j=0}^{\infty} (-1)^j \xi^{4j} \left( \frac{\sqrt{2\pi}}{(2j)!} \xi^3 - \frac{4^{2j+1} (2j)!}{(1+4j)!} \xi^4 + \frac{\sqrt{2\pi}}{(1+2j)!} \xi^5 \right) \quad (1)$$

in which

$$\xi = \lambda_1 i_x \quad (2)$$

$$\lambda_1 = \sqrt{\frac{K_s}{4E_1 I}} \quad (3)$$

$$K_s = \frac{12E_s R}{i_x} \quad (4)$$

Vorster *et al.* (2005) proposed that this method should be used in conjunction with an appropriate shear stiffness degradation to arrive at a representative soil stiffness value. Taking this into account along with the alternative subgrade modulus analogue proposed by Klar *et al.* (2005), overestimations of maximum bending moments were reduced by approximately 5–7 times for a volume loss of up to 4% as opposed to up to 20 times if the pipelines were forced to conform to greenfield settlement profiles.

While these numerical approaches have been shown to be very useful for pipeline assessments, none of these methods have been validated for tunnels. In the work reported in this paper, cross-sectional bending strains and longitudinal strains were investigated through field monitoring and centrifuge modelling.

Manuscript received 6 February 2017; revised manuscript accepted 19 June 2017. Published online ahead of print 19 July 2017.

Discussion on this paper closes on 1 February 2018, for further details see p. ii.

Published with permission by the ICE under the CC-BY license. (<http://creativecommons.org/licenses/by/4.0/>)

\* Department of Engineering, University of Cambridge, Cambridge, UK (Orcid:0000-0001-8882-4554).

† Department of Engineering, University of Cambridge, Cambridge, UK.

‡ Department of Civil Engineering, University of Berkeley, Berkeley, CA, USA.

**BOND STREET STATION UPGRADE (BSSU)**

*Background of BSSU and Royal Mail tunnel (RMT)*

The BSSU is part of Transport for London’s major upgrade plan for the London Underground. It aims to increase passenger capacity with a new ticket hall extension and 500 m tunnels linking to the platform tunnels of Crossrail and existing Central and Jubilee Lines. The lower access tunnel 4/207 (LAT) was constructed by means of open-faced tunnelling with sprayed concrete lining (SCL). The tunnel was located directly underneath the existing 3 m dia. cast-iron RMT with a 15° skew from a perpendicular undercrossing (see Fig. 1). The LAT is a squat elliptical tunnel with an equivalent circular diameter of 6.3 m that reduces to 5.78 m at the point of undercrossing where both tunnels are essentially in contact (i.e. zero clear distance).

The RMT was built in 1917 to convey mail between eastern and western sorting offices across London through a 10.5 km long driverless rail system. In 2003, the RMT was mothballed due to high running costs, presenting an excellent opportunity to access the tunnel for various instrumentation systems. The RMT was constructed wholly in London Clay, similar to the LAT, except for the invert which toes into the Lambeth Group (very stiff clay of upper mottled beds).

*Construction progress*

On average, a daily advancement of 1 m was achieved by means of the top and bench excavation method. The construction progress to be discussed here covered the

period from 10 November 2014, just before the construction of the LAT entered the influence zone of the RMT and before any appreciable response from the instrumentations, to 2 December 2014 when the construction had passed the centre-line of the RMT by approximately 1D. Baseline readings of all instruments were taken in October 2014. Fig. 2 shows the cross-sectional view of the tunnelling advance in relation to the RMT.

*Instrumentation*

*Distributed fibre optic strain sensing system (DFOS).* The DFOS capitalises on the linear relationship between strain and phase shift of backscattered light waves travelling through fibre optic cables to provide a continuous strain profile (Mohamad, 2008). Since it is based on an optical system, no electrical power is required with the exception of the analyser, which can be placed kilometres away from the instrumented section.

The layout and installation method of the DFOS in the RMT is conceptually similar to previous monitoring within the same tunnel at the Crossrail Liverpool Street station (Gue *et al.*, 2015), consisting of five cross-sections at rings R11010, R11022, R11027, R11032 and R11042 and a longitudinal pre-stressed section that spans 35 m from R10990 to R11060, as shown in Fig. 3.

Zero-strain loops were introduced between consecutive instrumented cross-sections, which were essentially 5 m loops of the fibre optic cable enclosed loosely within a box for

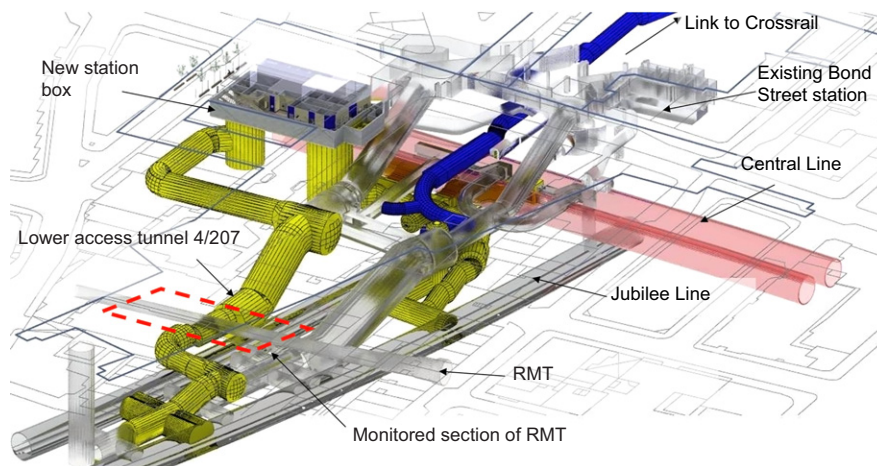


**Fig. 1. Underground 3D view of BSSU scope of works**

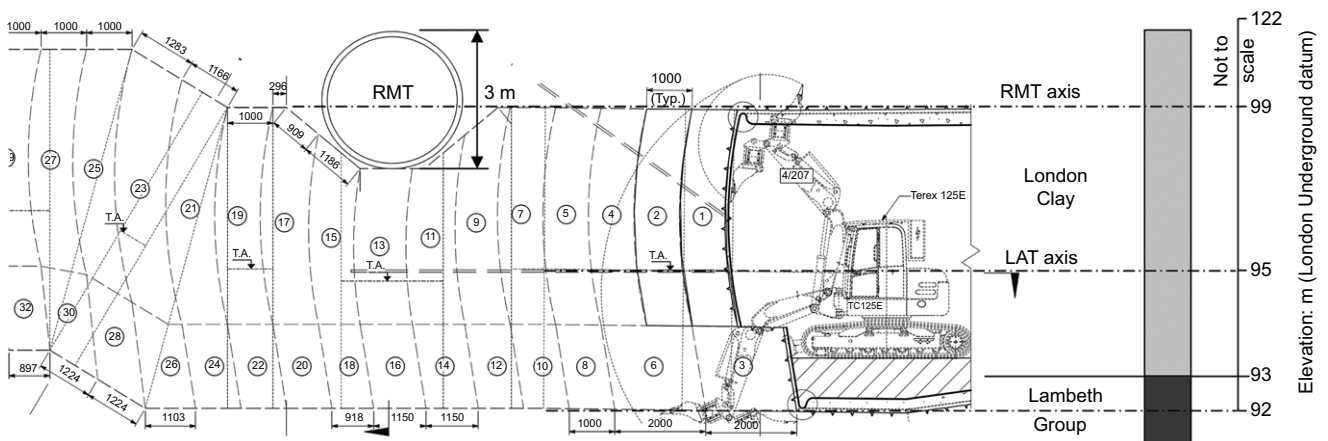


**Fig. 2. Cross-sectional view of tunnelling advance in relation to the RMT with soil profile**

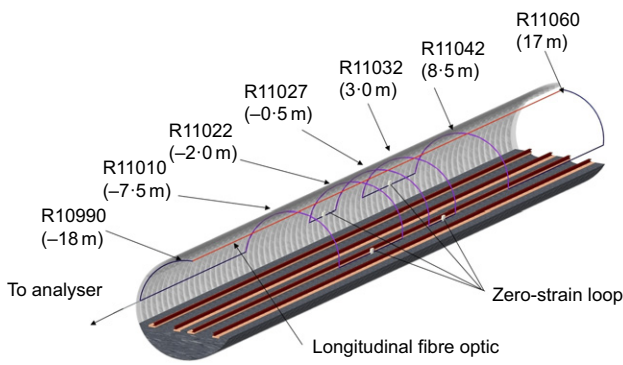


Fig. 3. Layout of DFOS cable in the RMT

protection. These served three functions: (a) providing a reference for thermal strain measurements, (b) preventing unwanted strain from unintentional movements during monitoring (i.e. dragged by power cables used for other monitoring systems) by incorporating additional slack and (c) providing an emergency length of cable to bypass damaged cable sections.

*Instrumented bolts and shear gauges.* Two types of vibrating wire sensor were installed in the RMT – instrumented bolts to measure strain in the tunnel connections and vibrating wire displacement transducers to measure differential vertical shearing of the tunnel rings at the circumferential joints.

A total of 11 grade 8.8 M20 × 140 mm instrumented bolts were installed along the crown of the tunnel between R11010 and R11038 with an additional five units to measure differential shearing between neighbouring tunnel rings, installed within the radial connections of R11027. Each of the instrumented bolts, designed especially for this research

project, was internally fitted with a miniature vibrating wire strain gauge.

In addition, four vibrating wire displacement shear gauges were installed along the north springline of the RMT at R11019, R11021, R11023 and R11025. The layout of the instrumented bolts and shear gauges is shown in Fig. 4.

*Sattar image tracking.* A new photogrammetric system, Sattar image tracking (SIT), was deployed to monitor movement of the existing tunnel linings. This system, based on the fundamentals of digital image correlation, uses off-the-shelf digital single-lens reflex cameras to track multiple pre-installed targets or natural features (Alhaddad, 2016). In this way it is possible to monitor a significantly larger number of points at high accuracy (sub-millimetre) while providing visual images that serve as an additional source of information (e.g. wet surfaces signifying water leakage as tunnel segments deform).

Three cameras (cameras 01, 02 and 03) were installed to measure tunnel convergence between four targets at the left axis, (LeAx), right axis (RiAx) axis, crown (Crwn) and right invert (RiIn) of each monitored ring. A plan view of the complete set-up is shown in Fig. 5.

*Field instrumentation results*

*Cross-sectional lining response (R11027).* The strain profile on the intrados provides a qualitative assessment of the deformation mode: a cosine-shaped profile with tension along both springlines and compression at the crown represents vertical ovalisation, while a sine profile denotes ovalisation with a skew (see Fig. 6).

Figure 7 shows the continuous intrados strain readings at R11027 of the RMT; the horizontal axis denotes distance along the cable (positive strain values represent tensile strains throughout this paper). Data are shown for two specific

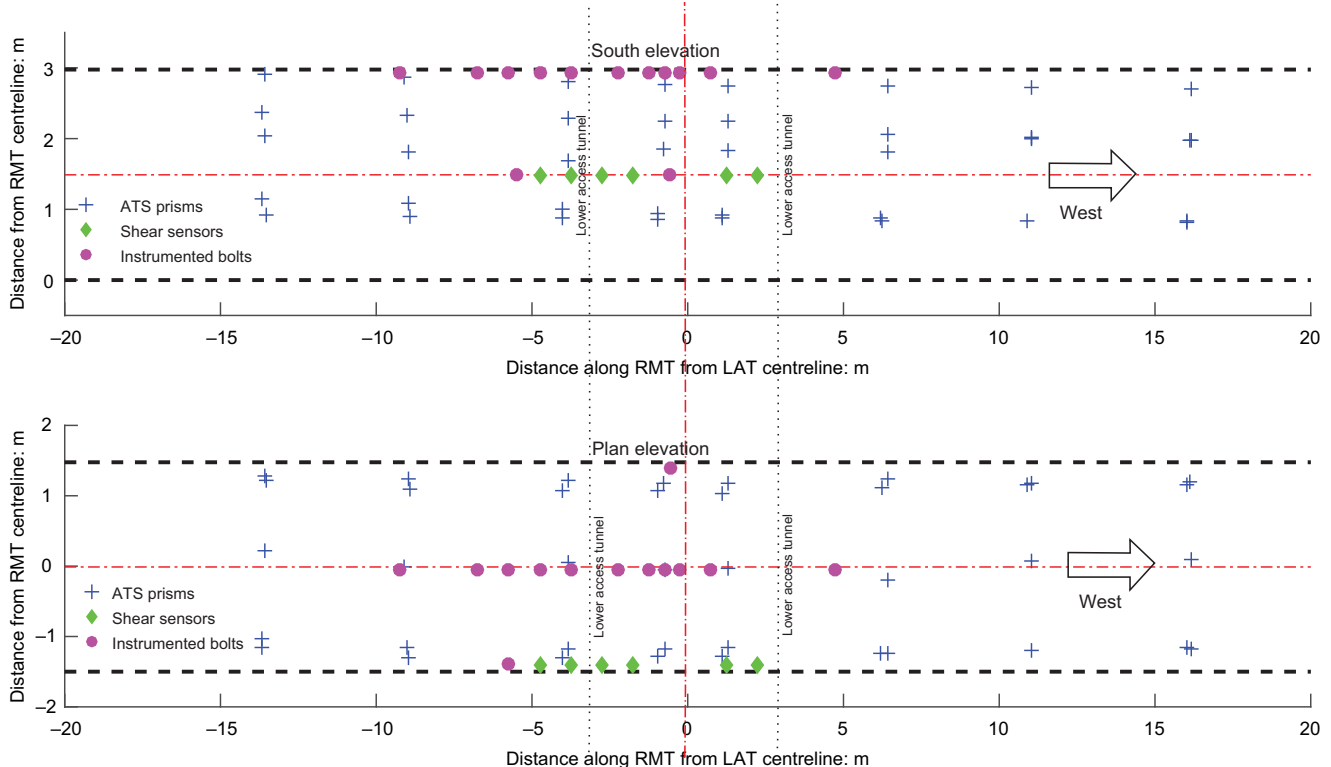


Fig. 4. Layout of instrumented bolts and shear sensors in the RMT

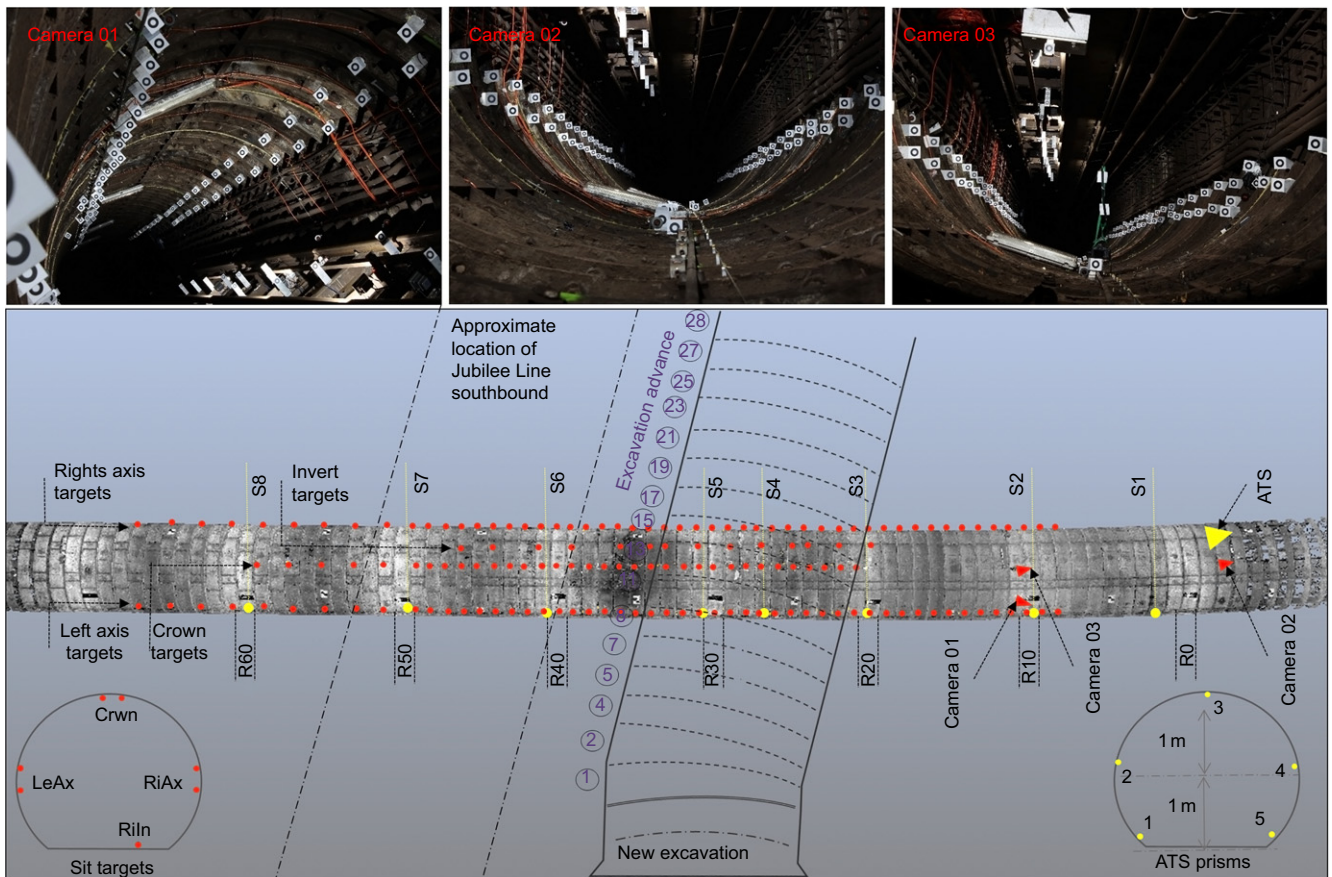


Fig. 5. SIT camera and target installation layout at the RMT

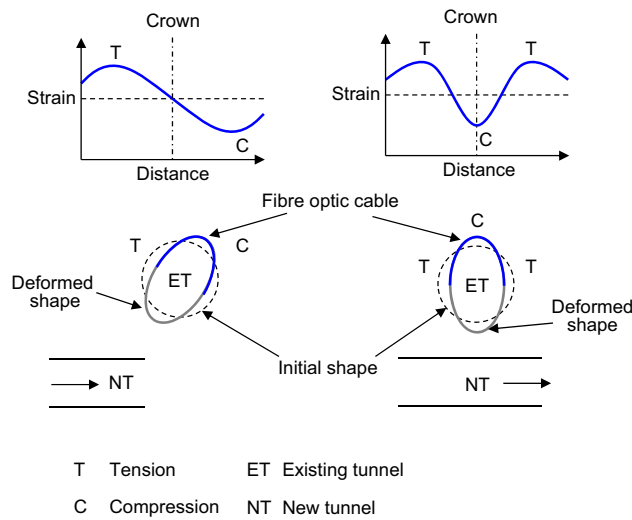


Fig. 6. Visualisation of deformation modes from DFOS strain profile in RMT

construction dates: 27 November 2014 (line with black dots) and 2 December 2014 (line with black squares), corresponding to the periods where the tunnelling face was directly below and 0.8D past the centre-line of R11027.

Skewed deformation was evident during the approach as a sine profile was observed, indicating that the invert of R11027 moved towards the tunnelling face due to stress relief when the magnitude of strain increased as the tunnelling face approached the RMT.

Due to the very close proximity of the two tunnels where the invert of the RMT was exposed during tunnelling, SCL was applied directly onto the extrados of the RMT invert, which restrained the cross-sectional deformation. This temporarily ‘locked’ the skewed ovalisation in place even when the invert of R11027 was excavated on 27 November 2014. This resulted in strains of approximately  $\pm 600 \mu\epsilon$  (0.06%) for the springlines and crown.

As the tunnelling face cleared the RMT, stress relief of the soil on the far side caused R11027 to deform and reach a new equilibrium when its profile took on the expected cosine shape for vertical ovalisation. The magnitudes of strains were reduced to  $\pm 290 \mu\epsilon$  (0.029%) by the time the final reading was taken on 2 December 2014. The asymmetrical final cosine strain profile indicated that a minor rotation remained with ovalisation towards the tunnelling approach, even after the tunnelling face had cleared the RMT.

Predictions from the mobilised strength design approach developed from the centrifuge test results showed good agreement with the measured strains for the springline. This will be discussed further in the section ‘Centrifuge modelling test results’.

The cross-sectional instrumented bolt data (Fig. 8) were in good agreement with the trend of strains indicated by the DFOS, albeit at a much lower strain level. The distance values on the horizontal axis of Fig. 8 are similar to those of Fig. 7, where positive values indicate tensile strains.

Maximum tensile strains of  $140 \mu\epsilon$  (0.014%) and  $42.4 \mu\epsilon$  (0.00424%) for the left and right wall respectively were recorded on 27 November 2014, when the tunnel face was directly below R11027, consistent with observations of the DFOS. The disparity in strain magnitudes from the

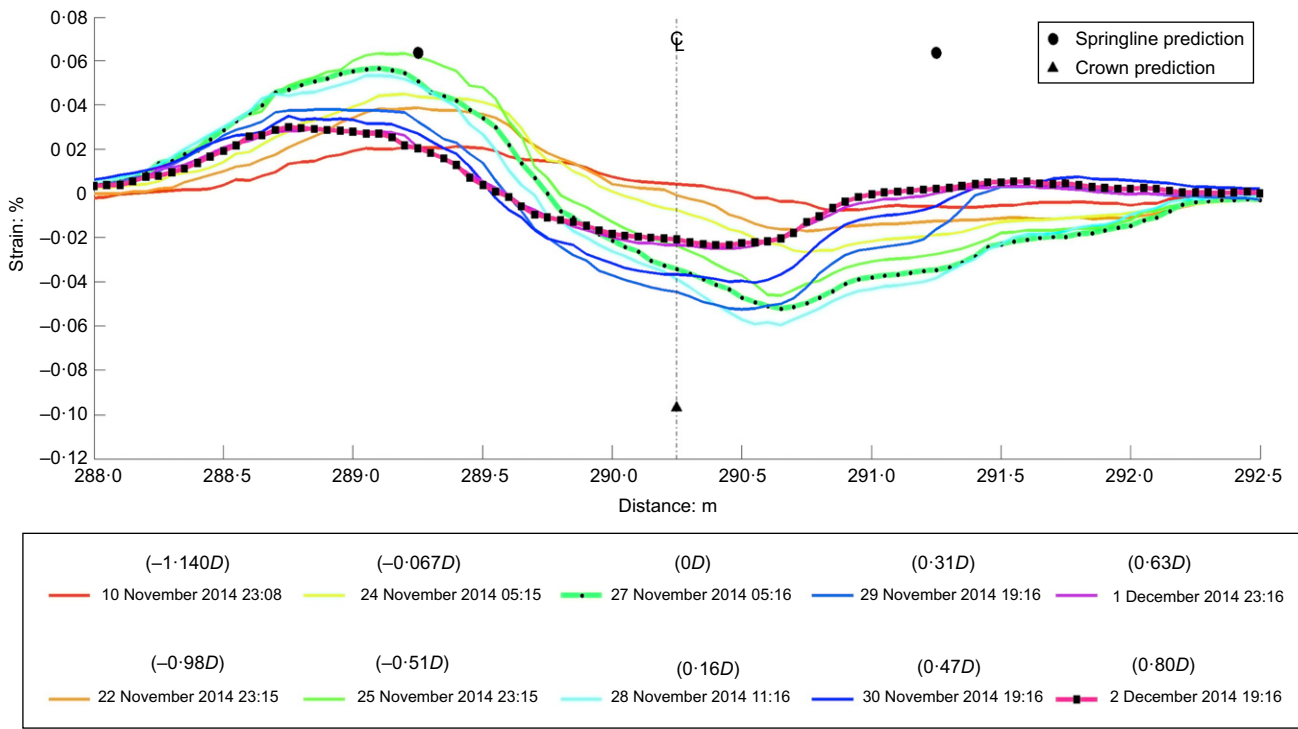


Fig. 7. Development of cross-sectional strains at intrados of R11027 of RMT. A full-colour version of this figure can be found on the ICE Virtual Library ([www.icevirtuallibrary.com](http://www.icevirtuallibrary.com))

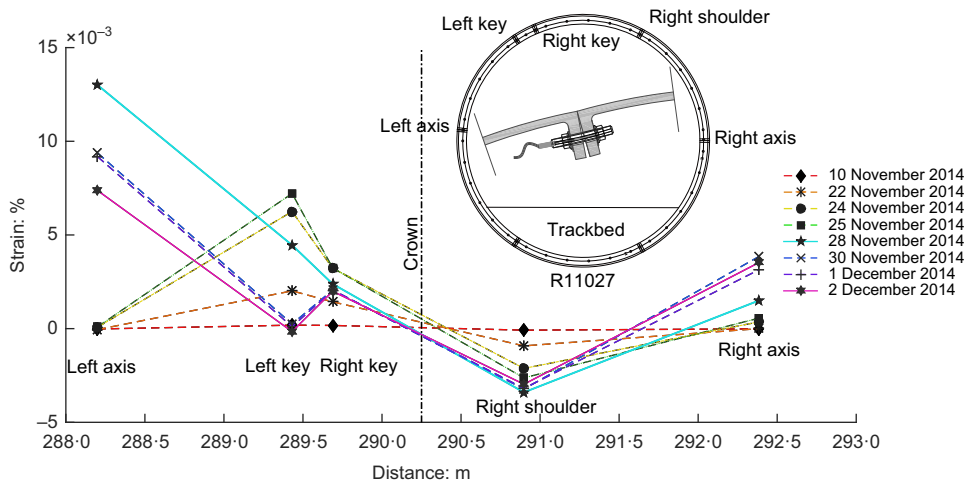


Fig. 8. Cross-sectional instrumented bolt data at R11027

instrumented bolts and the DFOS can be attributed to two factors. The first factor is the relative location of each system to the neutral axis – the instrumented bolts measured strain at a location approximately in the middle of the cross-section rather than on the internal surface as for the DFOS; the instrumented bolts were thus closer to the neutral axis of flexure. Secondly, the instrumented bolts measured the strain between the radial segment flanges, at a distance of approximately one fifth of the segment width from the circumferential flange, to which the DFOS was affixed. Distortion of the radial flanges (pivoting around the position of the instrumented bolt) and the circumferential flange (pivoting around the root) caused a further disparity in the strain regimes of the DFOS and instrumented bolts (Wilcock, 2017).

The results from both the DFOS and the instrumented bolts indicate that the RMT ovalisation reduced as the tunnelling works progressed, although the tunnel did not return to its virgin state but rather an oblique ovaloid.

Similar trends were observed from the SIT and conventional automated total station (ATS) prism data, as shown in Fig. 9. The relative convergence of R11027 was consistent with the deformation mode of the ring, which ovalised towards the tunnelling face during the approach. Very good agreement was observed between the SIT and ATS data throughout the monitoring period. A maximum convergence of approximately 11 mm (0.4%D) was observed for LeAx–RiIn when the tunnelling construction was directly below R11027, while the horizontal convergence of LeAx–RiAx was smaller at about 7 mm (0.25%D).

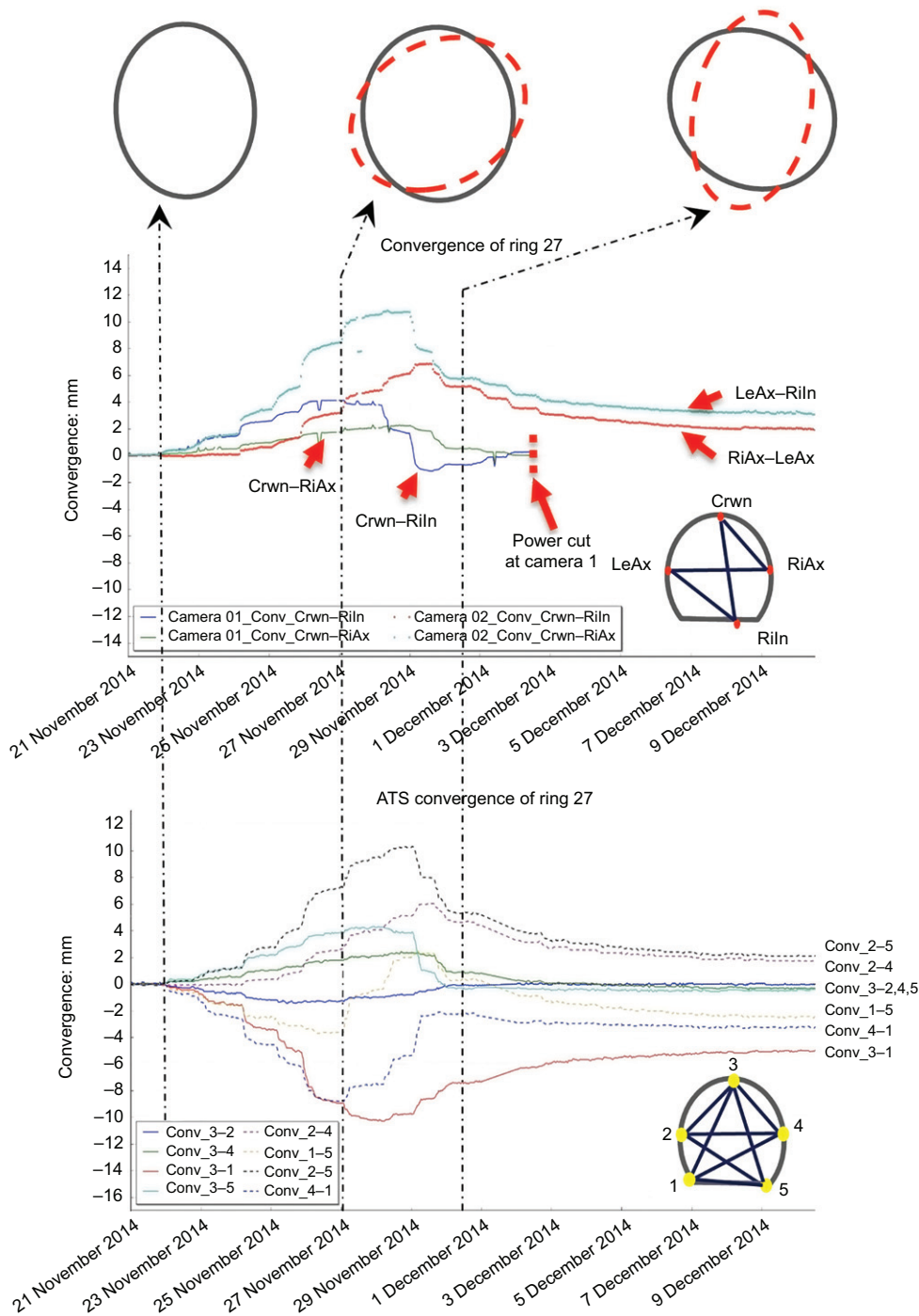


Fig. 9. SIT and ATS convergence data for R11027 (positive convergence is convergence measured across axes)

All four independent measurements of the SIT, ATS, instrumented bolts and DFOS showed agreement and indicated that the final deformed shape was not a perfect vertical ovalisation but was slightly rotated towards the tunnel approach. It is likely that application of the SCL directly onto the extrados of the RMT partially constrained its deformation.

*Longitudinal tunnel response.* The pre-strained DFOS cable along the crown measured longitudinal strains. The recorded data are shown in Fig. 10 in which the horizontal axis denotes the distance along the fibre optic cable and the left-hand side of the graph is to the east. Sagging strains were confined within  $\pm 0.8D$  from the centre-line of the new tunnel

at R11027, with the overall zone of influence within approximately  $\pm 2.5D$ .

Two sagging peaks can be observed at a distance of 330 m ( $0.4D$ ) and 332 m ( $0D$  at R11027). This is due to the  $15^\circ$  skewed alignment between both tunnels: the projected tunnelling face at a distance was aligned with the former point of 330 m ( $0.4D$ ) of the RMT while it gradually shifted to 332 m ( $0D$ ) as the tunnelling face approached and passed underneath the RMT, registering a maximum compressive strain of  $-737 \mu\epsilon$ .

The location of maximum tensile strains in the hogging region varied at  $-1.1D$  and  $1.6D$  from the centre-line of the LAT, with the larger value recorded on the west side. The magnitudes of maximum tensile strains in the west were, on average, 33% larger than those in the east, with a maximum

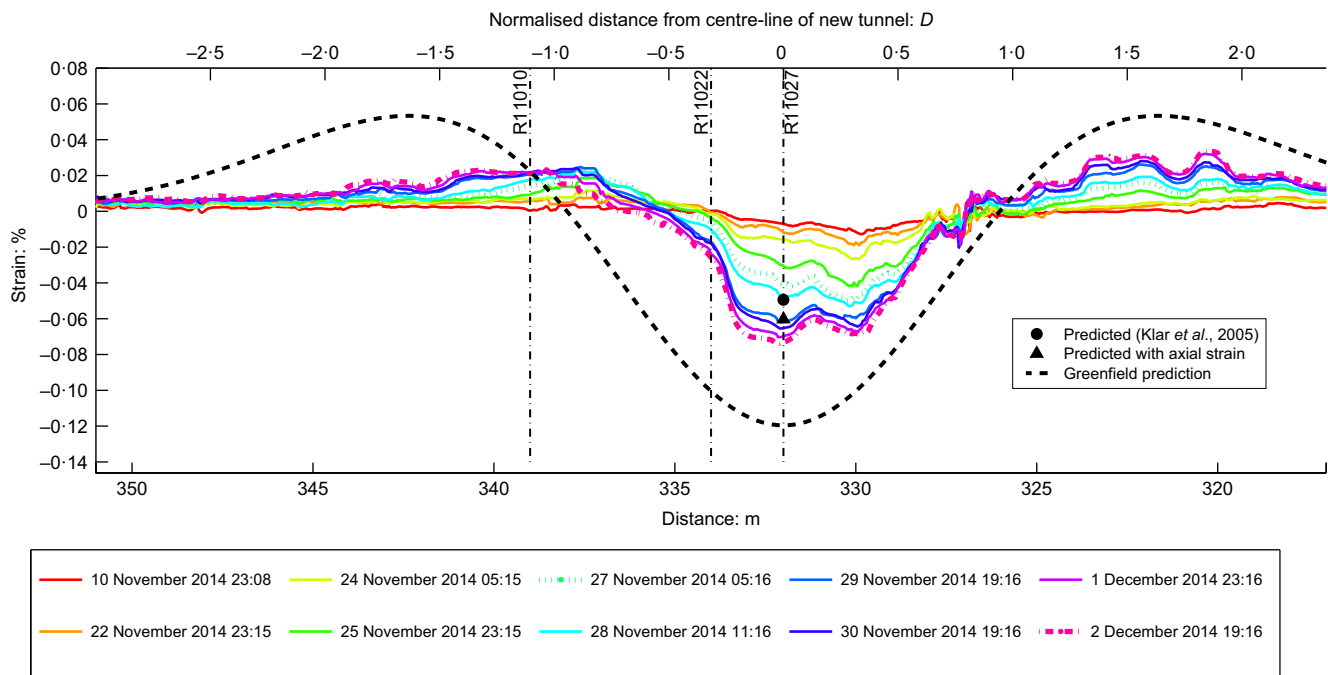


Fig. 10. Longitudinal strain response of the RMT from DFOS. A full-colour version of this figure can be found on the ICE Virtual Library ([www.icevirtuallibrary.com](http://www.icevirtuallibrary.com))

value of  $333 \mu\epsilon$ . The reason for this difference is the proximity to adjacent construction of access shafts and underpinning works for the BSSU towards the west, which would have strained the surrounding soil and reduced its stiffness.

The strain prediction, assuming that the RMT followed a greenfield settlement profile at the prescribed design volume loss of 1.5%, is shown as the dark broken curve in Fig. 10; the predicted curve overestimated both sagging and hogging strains by approximately 60%, ignoring any axial strain component. The measured strain profile was much narrower, indicating that its effects were localised.

Data from longitudinal instrumented bolts (Fig. 11) revealed comparable strain profiles but once again at a lower magnitude; the horizontal axis in Fig. 11 is identical to that used for the longitudinal DFOS data in Fig. 10. A maximum compressive strain of  $-135 \mu\epsilon$  ( $-0.0135\%$ ) in the sagging region was measured at R11028, at an offset of 0.5 m, while a maximum tensile strain of  $60 \mu\epsilon$  ( $0.006\%$ ) was recorded at a similar location.

If the tunnel segments were acting as rigid bodies, the instrumented bolts would be expected to have measured significantly larger strain values than those measured by the DFOS because the deformation was concentrated over a

much smaller distance. Since this was not the case, it is postulated that distortion of the circumferential flanges, similar to the radial flanges, had a strong influence on the relationship between the measurements from the two types of instrumentation. This reduced the amount of stresses carried by the bolts.

Given that the stiffness of the wrought-iron bolts was 190 GPa, the maximum induced tensile and compressive stresses based on the measured strains were 11.4 MPa and  $-25.65$  MPa, respectively. Residual loads in the existing bolts were also measured by replacing a number of existing bolts with an instrumented bolt that was re-tightened to restore the existing flange gap as measured by a dial test indicator prior to removing the existing bolt. The residual stresses had a median value of approximately 24 MPa (Wilcock, 2017).

It is interesting to note that the equivalent torque was relatively close to the recommended good-practice value of 50 Nm by London Underground Limited for new bolts, putting the residual tensile axial stress at approximately 40 MPa. Taking this into account, the final average axial bolt stresses would be 51.4 MPa and 14.35 MPa for the maximum measured tensile and compressive strains, respectively, keeping them well within the serviceable limit of 85.5 MPa.

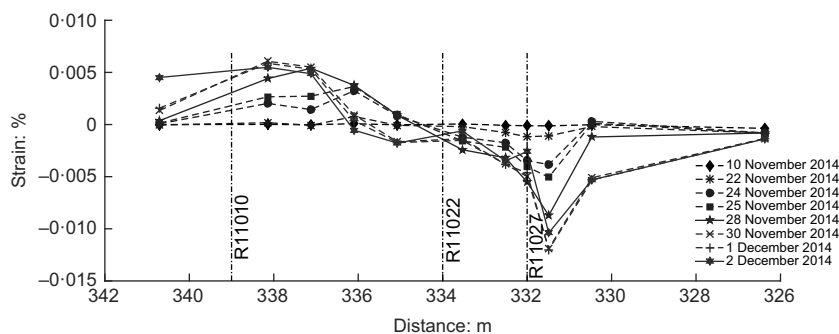


Fig. 11. Data of longitudinal instrumented bolts in RMT

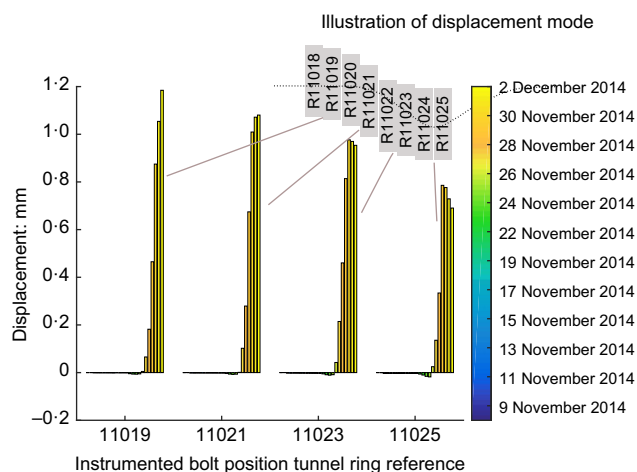


Fig. 12. Shear displacement sensor data from four instrumented rings in the RMT

Data from the shear displacement sensors (Fig. 12) indicate that the acting shearing was far less linear with respect to the position of the tunnel face; the effects of shearing were only measured when the tunnel face was effectively directly underneath the RMT. A maximum shearing displacement of 1.2 mm was recorded at R11019, which is approximately 5.0 m from the centre-line of the LAT. This is consistent with simple bending of a monolithic tube, in which maximum shear occurs at the point of minimum curvature.

By considering the position of peak shearing to be consistent with zero curvature (inflection), it is possible to extend the shearing data about the point of inflection such that a cumulative shear result can be obtained and the contribution of the potential shearing component to the overall settlement can be quantified. By performing this exercise for the four data points, the shearing contribution to vertical displacement of the RMT was determined to be approximately 30%.

The delay in the manifestation of shear suggests that the tunnel deformed through circle joint rotation (i.e. classical bending) until such a point where the radius of curvature became small, activating a shearing mechanism in which there was ring-to-ring slip such that settlements were further accommodated with little increase in longitudinal strain. The shear strains were thus released through ring-to-ring sliding movement rather than developing as strain within the tunnel segments.

## CENTRIFUGE MODELLING

In order to make comparisons with the collected field data, a series of three-dimensional (3D) centrifuge tunnelling tests in clay was carried out in the 10 m beam centrifuge of the Schofield Centre (Schofield, 1980). All tests were carried out at 100g to investigate the deformation mechanisms at realistic prototype-scale stresses.

Two tests were carried out (PP\_CYG\_C01 and PP\_CYG\_C03) with clear distances between two tunnels of

0.5D and 1.5D to investigate the difference in response at varying clear distances. The diameter of the existing tunnel was kept constant at 60 mm (equivalent to a 6 m dia. tunnel in prototype scale) along with a standard cover-to-diameter ratio for the existing tunnel of  $C/D = 1$ .

### Staged volume-loss tunnel model

As tunnelling is inherently a 3D process, an approximate 3D tunnelling model system was designed to simulate the tunnelling sequence of a 62 mm dia. tunnel in a series of five, 2D long advancements (Fig. 13). This system is an extension to the conventional plane-strain fluid extraction method used in previous centrifuge tests (e.g. Jacobsz, 2002; Vorster, 2005; Marshall, 2009; Williamson, 2013). Each fluid-filled section was isolated through individual solenoid valves; volume loss could be prescribed by extracting a precise volume of fluid from each section in series through internal drainage pipes. This variable control, along with the cleaner design with internal routing of pipes, minimises soil disturbance, which is a marked improvement over the system described by Boonyarak (2014).

### Tunnel lining bending instrumentation

The existing tunnel model was made from 60 mm (outer diameter) aluminium tube with a 1.5 mm wall thickness. A series of strain gauges was installed internally and externally to measure five longitudinal bending strains (DDL1–DDL5) and two instrumented cross-sections (R1 and R2) covered five bending strain sensing points, as shown in Fig. 14.

The ends of the tunnel were fixed for moment transfer while allowing 2 mm vertical translational movement for tunnel settlement during in-flight reconsolidation and tunnelling-induced settlements.

### Centrifuge package

A bespoke centrifuge package of internal dimensions 750 mm (width), 600 mm (length) and 440 mm (depth) was designed and built for this test series to minimise soil disturbance during model preparation (see Fig. 15). Assuming a trough width parameter  $K$  of 0.5, this effectively put the width of the package at a minimum of  $6.25i_x$ , beyond the  $5i_x$  influence zone recommended by O'Reilly & New (1982).

Speswhite kaolin clay was pre-consolidated at 1g to a maximum effective vertical stress of 400 kPa in the centrifuge package. This translated to overconsolidation ratios of 3 and 6 for the location of the new and existing tunnel axes, respectively. A series of plugs provided access to clay coring for the installation of tunnels, eliminating the need to remove the entire package wall and thus minimising soil disturbance.

### Centrifuge modelling test results

*Computation of shear strain based on the non-linear elastic-perfectly plastic (NLEPP) model.* Within generally achievable volume losses of up to 3% (Mair, 2008), shear strains around the existing tunnel were within the elastic range. The NLEPP model proposed by Vardanega & Bolton (2011)



Fig. 13. Fully assembled staged volume-loss tunnel model

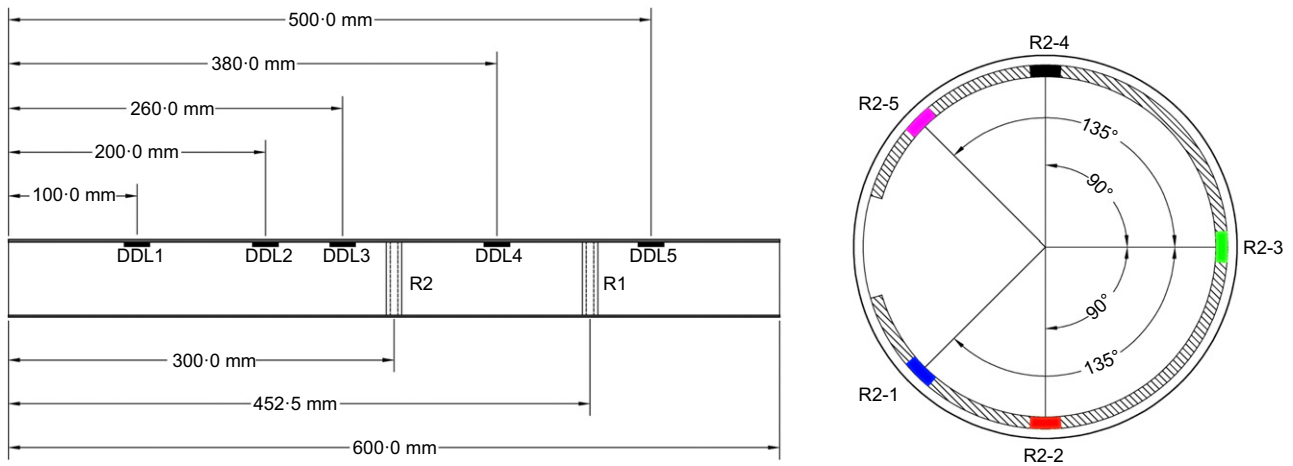


Fig. 14. Layout of instrumentation in existing tunnel model with sectional view of R2

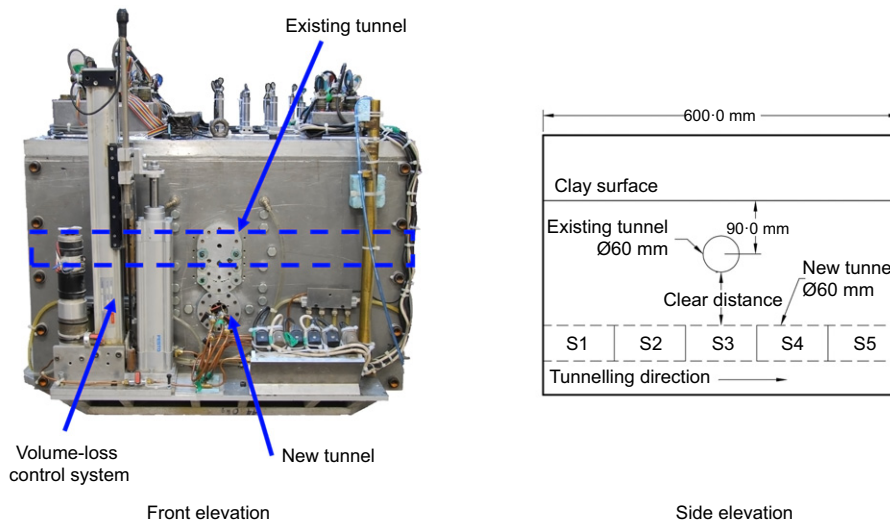


Fig. 15. Overall view of centrifuge package

based on a power law (equation (5)) was adopted to account for soil shear stiffness degradation in a simple manner.

$$\frac{\tau_{mob}}{c_u} = \alpha \gamma_{mob}^\beta \quad (5)$$

The regression and exponential coefficients  $\alpha$  and  $\beta$  can be determined from triaxial tests, in-situ pressure meter

stress–strain curves or through the relationship proposed by Vardanega *et al.* (2012) for Speswhite kaolin, which translates to  $\alpha$  and  $\beta$  values at the axis level for the existing tunnel of 3.279 and 0.436, respectively. Vardanega & Bolton (2011) suggested a  $\beta$  value of 0.6 for London Clay.

Tunnelling problems are often idealised as a cylindrical or spherical cavity contraction (see Fig. 16) with radial

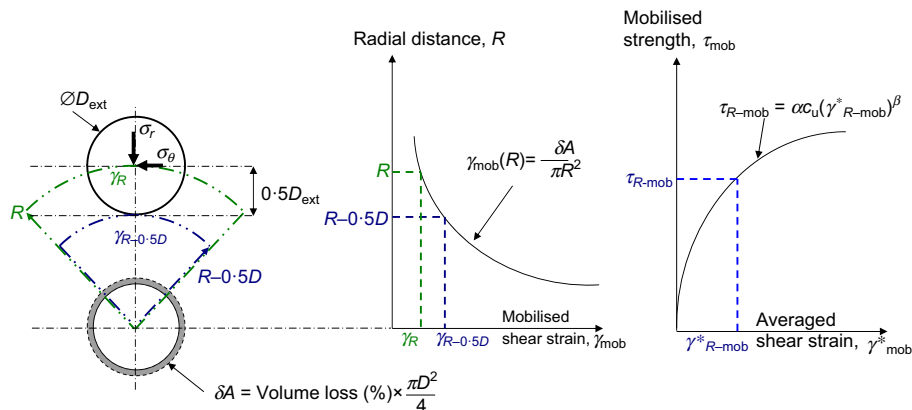


Fig. 16. Relationship between shear strain and radial distance from cavity contraction theory based on radial symmetry

symmetry (Mair, 2008). Hence, mobilised shear strain and subsequently mobilised shear stress can be calculated with knowledge of the volume loss and the radial distance away from the cavity. Thus, equation (5) is effectively

$$\frac{\tau_{\text{mob}}}{c_u} = \alpha \left( \frac{\delta A}{\pi R^2} \right)^\beta \quad (6)$$

Osman *et al.* (2006) presented a more rigorous method to evaluate shear strains for a single tunnel, which was derived from the greenfield Gaussian mechanism through work balance considerations. Radial symmetry provides a lower bound shear strain value while the method proposed by Osman *et al.* (2006) yields an upper bound value.

Taking into account that neither method was intended for evaluating soil strains with an additional existing tunnel in place, an alternative average shear strain assessment is proposed, utilising the concept of cavity contraction for simplicity.

Ghaboussi & Ranken (1977) and Boonyarak (2014) showed that major shear stress contours were concentrated within  $0.5D$  of an existing tunnel when a new tunnel was constructed in close proximity. Therefore, the average shear strain (see equation (7)) is calculated based on a simple average of shear strains calculated from radial symmetry at the point of consideration and a location  $0.5D$  below that point, as shown in Fig. 16, putting it between the upper and lower bound values. This is then converted to mobilised stress based on equation (7) with the appropriate  $\alpha$  and  $\beta$  values.

$$\gamma_{R-\text{mob}}^* = \frac{\gamma_R + \gamma_{R-0.5D}}{2} \quad (7)$$

$$\tau_{R-\text{mob}} = \alpha c_u (\gamma_{R-\text{mob}}^*)^\beta \quad (8)$$

**Cross-sectional bending moment.** Closed-form solutions for lining bending moments of a stand-alone tunnel have been developed by various researchers (Muir Wood, 1975; Duddeck & Erdmann, 1982; Bobet, 2001). While each solution incorporates various assumptions and degrees of complexity for the soil–structure interaction effects, all of them relate the ratio ( $M/r^2$ ) at a particular point in the tunnel lining to the difference between the vertical and horizontal stresses at the axis as

$$\frac{M}{r^2} = (\sigma_v - \sigma_h) \times \text{soil} - \text{structure interaction parameter} \quad (9)$$

It is worth noting that the cited methods of accounting for the soil–structure interaction were solely meant for stand-alone tunnels; however, the general philosophy can be applied to tunnelling under existing tunnels.

In order to identify the changes in vertical and horizontal stresses at the axis of the existing tunnel, a simple cavity contraction model can be utilised. Considering plane-strain geometry with the centres of the tunnels aligned vertically as shown in Fig. 16, the changes in vertical and horizontal stresses are similar to the changes in radial and tangential stresses. This stress difference is therefore equivalent to twice the mobilised strength of the soil for a given volume loss or shear strain.

$$\sigma_v - \sigma_h = 2\tau_{\text{mob}} \quad (10)$$

Substituting equation (10) into equation (8) gives

$$\frac{M}{r^2} = 2\tau_{\text{mob}} \times \text{soil} - \text{structure interaction parameter} \quad (11)$$

Based on results from both centrifuge tests, a linear correlation was obtained between the normalised bending moments ( $M/r^2$ ) and the mobilised stress for each of the critical locations of crown, springline and invert (see Fig. 17). The lines in Fig. 17 represent key locations on the existing tunnel lining (crown, springline and invert). Positive values denote hogging moments. Therefore, the existing tunnel ovalised vertically as the new tunnel was excavated directly below it, regardless of the magnitude of the clear distance.

Comparison was made with R11027 of the RMT, which sits directly above the new LAT tunnel; the results in Fig. 17 show good agreement for the left springline and crown. Bending moments for R11027 were back-calculated from intrados strain measurements based on simple beam theory with the assumption of negligible change in hoop strains (i.e. the neutral axis is unchanged from basic sectional analysis). A similar approach was used to convert the predicted bending moments from Fig. 17 into the intrados strains plotted in Fig. 7.

The normalised bending moment of the left springline was less than 5% above the predicted value while it overpredicted for the right springline. This disparity is due to the unique construction alignment and construction sequence described previously in the section ‘Cross-sectional lining response (R11027)’. However, the close prediction suggests that the cross-sectional response of the RMT lining was relatively rigid despite its segmental nature.

The predicted normalised bending moment of the crown was approximately 50% larger in comparison with the field data. This was due to the increased stiffness of the key segment near the crown along with contributions from the concrete invert, neither of which were modelled in the centrifuge tests.

Nonetheless, this approach effectively allows tunnelling-induced cross-sectional bending moment assessments to be carried out with reasonable accuracy for any known tunnel diameter and assumed volume loss, and for any clear distance between tunnels.

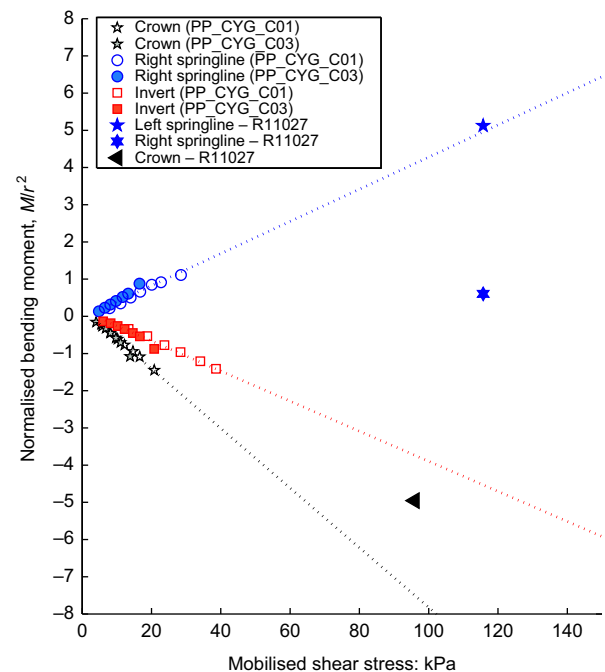


**Fig. 17. Relationship between cross-sectional normalised bending moments and mobilised stress**

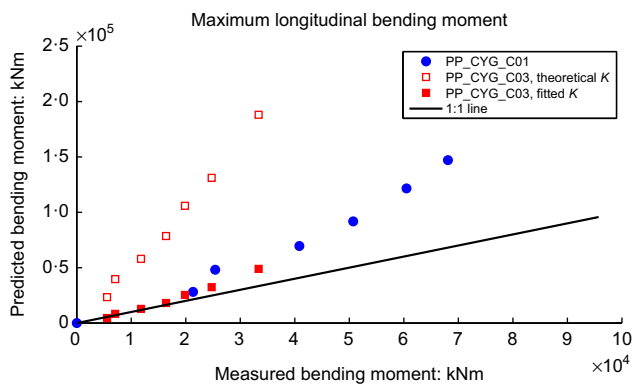


Fig. 18. Comparison of predicted maximum longitudinal bending moments using the method of Klar *et al.* (2005) with measured values from centrifuge tests

**Longitudinal bending moment.** The centrifuge tests carried out validated the method proposed by Klar *et al.* (2005) for tunnels in clay with shear stiffness degradation based on the NLEPP model (see Fig. 18). In line with the observations of Vorster *et al.* (2005), the method overpredicts the measured maximum bending moments by a factor of 1.9 to 5.1. Better agreement was found for the case of the smaller clear distance between the two tunnels (0.5D) as it resulted in bending strains that were more consistent with the Gaussian profile. A fitted  $K$  value back-calculated from the bending strains provided a better fit for PP\_CYG\_C03 (1.5D clear distance), reducing the difference from a factor of 5.1 to 1.2. It should be noted that, although the resultant curve fit was poor, the objective of the exercise was to illustrate the applicability of the method proposed by Klar *et al.* (2005) when the tunnel deformation profile conforms to a Gaussian curve, a trend that is generally observed from field instrumentations (Standing & Selman, 2001; Gue *et al.*, 2015).

Two possible explanations are proposed for the wider settlement trough measured in PP\_CYG\_C03. Firstly, it is possible that the tunnelling-induced loading at the larger clear distance was sufficiently small that the stiff existing tunnel model responded as a beam. Alternatively, as volume loss was triggered directly below the existing tunnel, the soil above could move around its circular profile and into the cavity of the new tunnel, forming a static wedge directly below the invert of the existing tunnel. This is comparable to the movement of soil around a circular pile, as described by Randolph & Houlsby (1984) and subsequently by Martin & Randolph (2006), where static wedges form at both the leading and trailing edges of a circular pile.

At very small clear distances of 0.5D, shear strains were sufficiently large to induce block failure, thus preventing the formation of a static wedge. However, in the case of PP\_CYG\_C03 (with a clear distance of 1.5D), the formation of a static wedge is possible. This static wedge could have provided some amount of soil support over the new tunnel, thus widening the settlement profile of the existing tunnel.

Although particle image velocimetry (PIV) was not possible in this test series, the effect of the static wedge was further supported by the development of compressive hoop strains in the existing tunnel and a significant increase in bending strains at the knees instead of the invert. This observation would be less likely to occur in the case of beam action. Nonetheless, proof of its formation along with the conditions of formation (correlation to surface roughness factor etc.) along with the amount of support provided would require further research, and neglecting its effect would be conservative.

**Longitudinal axial strain component.** Theoretical greenfield horizontal ground movements were derived from the vertical components (assuming ground movement vectors were directed towards the centre of the new tunnel). Occlusion of an existing tunnel creates a condition where soil settles less directly above the longitudinal direction of the existing tunnel and settles more to the side of it. Thus, without any subsurface soil data such as those obtained from PIV, the greenfield horizontal strain that was induced is inconclusive.

An alternative method of applying a reduction factor to the measured longitudinal curvature strains rather than to the greenfield horizontal strains is suggested. Longitudinal curvature strain is defined as the bending strain for a structural element with its neutral axis located at mid-depth. Since curvature strains represent the vertical settlements of the existing tunnel, application of a reduction factor to the measured curvature strains is conceptually comparable to the method proposed by Bracegirdle *et al.* (1996).

The reduction factor in both tests was 15–30% of the curvature strain, with an average of 20%, irrespective of volume loss. It should be noted, however, that surface roughness plays a part in the amount of the axial component that is transferred from the soil to the tunnel. The average of the curvature strains (20%) was obtained for a smooth aluminium tunnel model. Further research is required to ascertain the effect of various surface roughness factors on the reduction factor.

The predicted strains at the crown level of the RMT are compared with the DFOS-measured values in Fig. 10. Strains were back-calculated from predicted bending moments calculated using the method proposed by Klar *et al.* (2005) with the soil stiffness estimated from the NLEPP model at the axis of the existing tunnel. The resulting strain (the circle symbol in Fig. 10) underpredicted the maximum sagging strain, with a value of  $-426 \mu\epsilon$ . However, application of a reduction factor of 20% for the axial component yielded a strain of  $-519 \mu\epsilon$  (triangle symbol in Fig. 10), closing the gap with the measured value with an underprediction of strain by 30%.

Similar to the case of cross-sectional strains, it would be expected that the measured longitudinal strain would exceed predictions since the caulking between consecutive rings are compressible, therefore reducing compressive stiffness and allowing the existing tunnel to respond flexibly in the longitudinal direction, in line with the observations of Standing & Selman (2001). Thus, the predicted values, which assume a continuous lining, would be conservative for segmental tunnel lining behaviour.

## CONCLUSIONS

Approximate 3D tunnelling simulations were carried in clay using novel centrifuge modelling techniques. The results were in good agreement with field data obtained from various state-of-the-art instrumentation systems. Based on the field data and centrifuge modelling results, the following conclusions can be drawn.

- The magnitudes of bending moments in the longitudinal direction were larger in comparison with cross-sectional values, thus making these more critical for assessment for a perpendicular undercrossing.
- The longitudinal deformation mode of the RMT was found to be a combination of both bending and shearing, with the former being dominant.

- (c) The existing segmental cast-iron lining of the RMT responded more flexibly in the longitudinal direction than in cross-section due to compressible caulking between consecutive rings.
- (d) Radial and circumferential flanges of cast-iron segments distorted to accommodate bending deformation, which reduced the strains within the bolt connections.
- (e) Good transferability of the pipeline assessment method proposed by Klar *et al.* (2005) was confirmed by both centrifuge and field data with the inclusion of an axial component.
- (f) A mobilised strength design approach was proposed to evaluate bending moments based on cavity contraction theory. This method allows a quick assessment with minimal input parameters to yield realistic cross-sectional bending moments.

#### ACKNOWLEDGEMENTS

This research would not have been possible without financial support from Laing O'Rourke plc for the first author's PhD studentship. The authors would also like to acknowledge the logistical and technical support provided by London Underground, Royal Mail Group Ltd, CH2M Hill and the Schofield Centre technicians and the continuous support from the UK Engineering and Physical Sciences Research Council (EPSRC) and Innovate UK through their funding of the Cambridge Centre for Smart Infrastructure and Construction (CSIC).

#### NOTATION

$c_u$	undrained shear strength
$D$	tunnel diameter
$E_l$	Young's modulus of tunnel lining
$E_s$	Young's modulus of soil
$I$	second area moment of inertia
$i_x$	inflection point of transverse settlement curve at depth of interest
$K$	trough width parameter
$K_s$	soil subgrade modulus
$M$	cross-sectional bending moment
$M_{\max}$	maximum longitudinal bending moment
$R$	radial distance from centre of new tunnel to point of interest
$r$	radius of existing tunnel
$S_{\max}$	maximum greenfield soil settlement at depth of interest
$\alpha$	regression coefficient for non-linear elastic-perfectly plastic (NLEPP) model
$\beta$	exponential of regression analyses for NLEPP model
$\gamma_{\text{mob}}$	mobilised shear strain
$\delta A$	reduction in area from volume loss
$\lambda_1$	relative structure-soil subgrade stiffness coefficient
$\sigma_v$	vertical stress
$\sigma_h$	horizontal stress
$\tau_{\text{mob}}$	mobilised shear strength

#### REFERENCES

- Alhaddad, M. M. (2016). *Photogrammetric monitoring of cast-iron tunnels and applicability of empirical methods for damage assessment*. PhD thesis, University of Cambridge, Cambridge, UK.
- Attewell, P. B., Yeates, J. & Selby, A. R. (1986). *Soil movements induced by tunnelling and their effects on pipelines and structures*. New York, NY, USA: Chapman & Hall.
- Bobet, A. (2001). Analytical solutions for shallow tunnels in saturated ground. *J. Engng Mech.* **127**, No. 12, 1258–1266.
- Boonyarak, T. (2014). *Three-dimensional interaction of multiple crossing tunnels: centrifuge and numerical modelling*. PhD thesis, Hong Kong University of Science and Technology, Clear Water Bay, Hong Kong.
- Bracegirdle, A., Mair, R. J., Nyren, R. J. & Taylor, R. N. (1996). A methodology for evaluating potential damage to cast iron pipes induced by tunnelling. In *Geotechnical aspects of underground construction in soft ground* (eds R. J. Mair and R. N. Taylor), pp. 659–664. Rotterdam, the Netherlands: Balkema.
- Duddeck, H. & Erdmann, J. (1982). Structural design models for tunnels. In *Proceedings of tunnelling '82* (ed. M. J. Jones), pp. 83–91. London, UK: The Institution of Mining and Metallurgy.
- Ghaboussi, J. & Ranken, R. E. (1977). Interaction between two parallel tunnels. *Int. J. Numer. Analyt. Methods Geomech.* **1**, No. 1, 75–103.
- Gue, C. Y., Wilcock, M., Alhaddad, M. M., Elshafie, M. Z. E. B., Soga, K. & Mair, R. J. (2015). The monitoring of an existing cast iron tunnel with distributed fibre optic sensing (DFOS). *J. Civ. Struct. Health Monitor.* **5**, No. 5, 573–586.
- Jacobsz, S. W. (2002). *The effects of tunnelling on piled foundations*. PhD thesis, University of Cambridge, Cambridge, UK.
- Kim, S. H. (1996). *Model testing and analysis of interactions between tunnels in clay*. DPhil thesis, University of Oxford, Oxford, UK.
- Klar, A., Vorster, T. E. B., Soga, K. & Mair, R. J. (2005). Soil-pipe interaction due to tunnelling: comparison between Winkler and elastic continuum solutions. *Géotechnique* **55**, No. 6, 461–466, <http://dx.doi.org/10.1680/geot.2005.55.6.461>.
- Mair, R. J. (2008). Tunnelling and geotechnics: new horizons. *Géotechnique* **58**, No. 9, 695–736, <http://dx.doi.org/10.1680/geot.2008.58.9.695>.
- Marshall, A. M. (2009). *Tunnelling in sands and its effect on pipes and piles*. PhD thesis, University of Cambridge, Cambridge, UK.
- Martin, C. M. & Randolph, M. F. (2006). Upper-bound analysis of lateral pile capacity in cohesive soil. *Géotechnique* **56**, No. 2, 141–145.
- Mohamad, H. (2008). *Distributed optical fibre strain sensing of geotechnical structures*. PhD thesis, University of Cambridge, Cambridge, UK.
- Muir Wood, A. M. (1975). The circular tunnel in elastic ground. *Géotechnique* **25**, No. 1, 115–127, <http://dx.doi.org/10.1680/geot.1975.25.1.115>.
- O'Reilly, M. P. & New, B. M. (1982). Settlements above tunnels in the United Kingdom – their magnitude and prediction. In *Proceedings of tunnelling '82* (ed. M. J. Jones), pp. 55–64. London, UK: The Institution of Mining and Metallurgy.
- Osman, A. S., Bolton, M. D. & Mair, R. J. (2006). Predicting 2D ground movements around tunnels in undrained clay. *Géotechnique* **56**, No. 9, 597–604, <http://dx.doi.org/10.1680/geot.2006.56.9.597>.
- Randolph, M. F. & Houlsby, G. T. (1984). The limiting pressure on a circular pile loaded laterally in cohesive soil. *Géotechnique* **34**, No. 4, 613–623, <http://dx.doi.org/10.1680/geot.1984.34.4.613>.
- Schofield, A. N. (1980). Cambridge geotechnical centrifuge operations. *Géotechnique* **30**, No. 3, 227–268, <http://dx.doi.org/10.1680/geot.1980.30.3.227>.
- Standing, J. R. & Selman, R. (2001). The response to tunnelling of existing tunnels at Waterloo and Westminster. In *Building response to tunnelling: case studies from construction of Jubilee Line Extension, vol. 2, case studies* (eds J. B. Burland, J. R. Standing and F. M. Jardine), pp. 509–546. London, UK: Thomas Telford.
- Vardanega, P. J. & Bolton, M. D. (2011). Strength mobilization in clays and silts. *Can. Geotech. J.* **48**, No. 10, 1485–1503.
- Vardanega, P. J., Lau, B. H., Lam, S. Y., Haigh, S. K., Madabhushi, S. P. G. & Bolton, M. D. (2012). Laboratory measurement of strength mobilisation in kaolin: link to stress history. *Géotech. Lett.* **2**, No. 1, 9–15, <http://dx.doi.org/10.1680/geolett.12.00003>.
- Vesic, A. B. (1961). Beams on elastic subgrade and Winkler's hypothesis. In *Proceedings of the 5th international conference on soil mechanics and foundation engineering*, vol. 1, pp. 845–850. Paris, France: Dunod.

- Vorster, T. E. B. (2005). *The effects of tunnelling on buried pipes*. PhD thesis, University of Cambridge, Cambridge, UK.
- Vorster, T. E. B., Klar, A., Soga, K. & Mair, R. J. (2005). Estimating the effects of tunnelling on existing pipelines. *ASCE J. Geotech. Geoenviron. Engng* **131**, No. 11, 1399–1410.
- Wilcock, M. J. (2017). *The behaviour of existing segmental cast iron tunnel linings subject to ground movement from new tunnelling*. PhD thesis, University of Cambridge, Cambridge, UK.
- Williamson, M. G. (2013). *Tunnelling effects of bored piles in clay*. PhD thesis, University of Cambridge, Cambridge, UK.